S1 Computed tomography (CT) scanning of a sediment core collected in lakes K and G, Bylot Island, Nunavut, Canada

To further investigate the cryostratigraphic characteristics of the ice and lake sediments, all samples were observed under X-ray computed tomography (CT) scanning (Siemens SOMATOM Sensation 64) at INRS- ETE (Quebec City, Canada), as in Calmels and Allard (2004). This technique relies on the calculation of the linear attenuation coefficient that measured the density of an object passed through an X-ray beam at different angles (Boespflug et al., 1994). A CT-scan produces cross-sectional images (usually 512 by 512 pixels matrix) of an object where each pixel of the image is assigned an X-ray attenuation value (μ), also called a CT number. CT numbers are then standardized using the Hounsfield scale, where the radiodensity of water (μ_{water}) is arbitrarily defined as 0 HU (Hounsfield units) according to Equation 1 (Hounsfield, 1973). Different shades of gray are assigned specific CT numbers to create the displayed image using a specific image processing software (Fiji) dedicated to DICOM (Digital Imaging and Communications in Medicine) images. In permafrost samples, unconsolidated sediments and rock (high density minerals) appear white, as the attenuation of these materials is very high. Gas inclusions and water appear black and other materials, such as ice, can have various shades of grey depending on their density.

$$\text{HU value} = \frac{\mu - \mu_{water}}{\mu_{water}} \times 1000\,, \quad (1)$$

This tool helps refine cryostratigraphic characterization of permafrost cores as it can reveal characteristics otherwise difficult or even impossible to observe with the naked eye. It allows visualization and characterization of the internal components and structures of the frozen sample, such as ice, grain-size variations, layer orientation in space, and gas inclusions. From a quantitative perspective, it has been used to segment images into regions of ice, gas and sediment in order to quantify the volumetric content of the scanned sample (Calmels et al., 2010; Dillon et al., 2008). Images were processed with FIJI to map X-ray attenuation coefficients on longitudinal images and to visualize sedimentary structures. The resulting images are displayed in greyscale, with darker grey representing a lower X-ray attenuation. Greyscale values are expressed as CT numbers, which are complex units related to the mineralogy, organic matter content, grain size, and bulk density.

References

Boespflug, X., Ross, N., Long, B., and Dumais, J. F.: Tomodensitométrie axiale: relation entre l'intensité tomographique et la densité de la matière, Canadian Journal of Earth Sciences, 31, 426-434, doi: 10.1139/e94-039, 1994.

Calmels, F., and Allard, M.: Ice segregation and gas distribution in permafrost using tomodensitometric analysis, Permafrost and Periglacial Processes, 15, 367-378, doi: 10.1002/ppp.508, 2004.

Hounsfield, G. N.: Computerized transverse axial scanning (tomography): Part 1. Description of system, The British Journal of Radiology, 46, 1016-1022, doi: 10.1259/0007-1285-46-552-1016, 1973.

S2 Bathymetric mapping through lake ice with ground-penetrating radar (GPR)

The difference between the dielectric properties of ice, water, and the sediments under lake bottoms makes GPR an effective method for determining lake depth profiles in the field. In this study, we used a pulseEKKO PRO controller manufactured by Sensors and Software coupled with 100 megahertz (MHz) antennas to obtain depth profiles from lake K and lake L. GPR profiles were calibrated and correlated with water depth measurements. Profiles were post-processed using Sensor and Software EKKO Project Version 5 proprietary software. Post-processing included time-zero correction and integration of GPS data, topography, and horizontal filtering to improve visualization of horizontal reflectors.

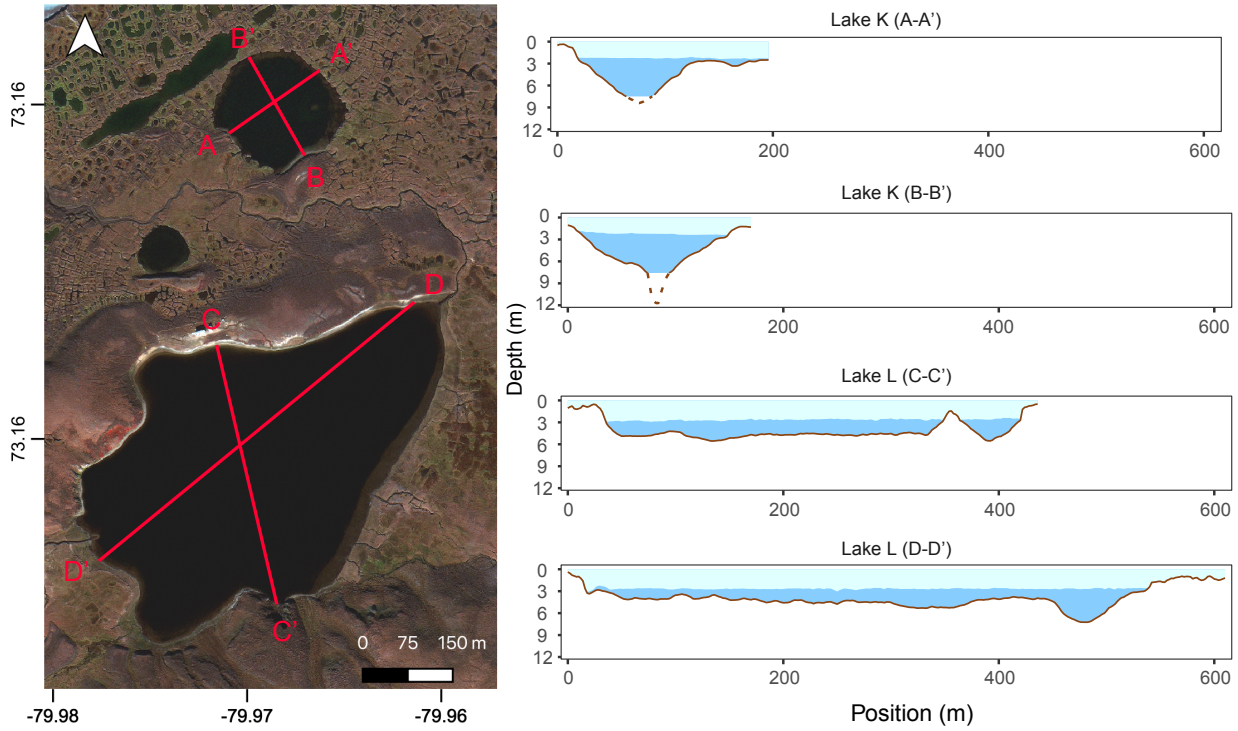

Figure S2: Ground penetrating radar profile of lakes K and L (background: GeoEye, 2010)

References

Moorman, B. J.: Ground-Penetrating Radar Applications in Paleolimnology, Vol. 1: Basin Analysis, Coring, and Chronological Techniques, in: Tracking Environmental Change Using Lake Sediments, edited by: Smol, J. P. and Last, W. M., Springer Netherlands, 23–47, 200.

Paquette, M., Fortier, D., Mueller, D. R., Sarrazin, D., and Vincent, W. F.: Rapid disappearance of perennial ice on Canada's most northern lake, Geophys. Res. Lett., 42, 1433– 1440, https://doi.org/10.1002/2014GL062960, 2015.

Table S3: Characteristics of lakes (n=21) for which bathymetric data were collected in 2015

Zone	Lake	Latitude	Longitude	Surface Elevation (m a.s.l.)	Max. depth (m)	Depth - Basin (m)		Depth - Platform (m)		Area (m^2)	Perimeter (m)	Shoreline development	Elongation index	Distance to glacier margin (m)
						Mean	Std. dev.	Mean	Std. dev.					
1	A	73.153	-80.034	7.1	2.9	1.5	0.4	1.2	0.3	6470.4	952.6	3.3	0.8	1505
	B	73.152	-80.030	7.1	3.2	2.0	0.6	1.1	0.3	19367.8	1111.2	2.3	1.5	1444
	C	73.153	-80.026	7.0	2.4	1.5	0.4	0.9	0.2	30968.2	709.7	1.1	0.4	1280
	D	73.151	-80.021	8.8	2.8	1.9	0.5	1.2	0.3	115306.2	1689	1.4	1.2	1197
	E	73.153	-80.019	7.0	3.3	2.2	0.6	0.9	0.2	37549.1	926.7	1.3	0.6	1064
	F	73.156	-80.006	7.7	4.3	2.3	0.6	1.7	0.2	18379.7	873.3	1.8	1	560
	G	73.153	-79.999	8.4	4.1	2.9	0.8	1.3	0.4	10076.6	694.9	2	1.2	464
	H	73.157	-80.000	5.7	2.5	1.5	0.3	0.8	0.2	34167	790.5	1.2	0.8	329
	I	73.160	-79.973	8.3	3	1.5	0.3	1.1	0.2	11501.6	790.1	2.1	3.8	586
	J	73.158	-79.974	6.8	6.1	1.8	0.3	1.0	0.2	5264.5	272.9	1.1	0.7	491
	K	73.160	-79.968	7.9	12.2	5.4	1.5	3.6	1.0	5226.1	447.4	1.7	1.6	748
	L	73.155	-79.969	8.2	11.7	4.7	2.0	2.2	0.6	209426.6	1991.9	1.2	1.1	514
2	M	73.185	-79.870	15.1	8.4	4.2	1.8	1.6	0.4	12963.4	695.3	1.7	1.1	1726
	N	73.190	-79.848	15.1	9.4	4.7	2.1	0.8	0.2	59699.7	1190	1.4	1.1	868
	O	73.191	-79.836	18.3	9.8	5.0	2.1	2.4	0.3	35566.3	2673.8	4	0.8	441
	P	73.192	-79.849	16.9	2.3	1.5	0.5	0.5	0.1	5354.2	403.7	1.6	1.7	768
	Q	73.193	-79.847	17.0	1.8	1.4	0.3	0.8	0.2	1292.5	139.8	1.1	1	674
	R	73.183	-79.872	14.2	3.9	2.6	0.8	0.9	0.2	22894.5	817.8	1.5	0.7	1873
3	S	73.153		354.0	15.4	6.9	4.0	1.0	0.3	54464.4	944.1	1.1	1	256
	T	73.144	-79.554	346.5	5.9	2.6	1.4	0.9	0.3	12754.9	446.4	1.1	0.6	829
	U	73.144	-79.531	359.4	4.3	2.6	1.0	1.2	0.3	9757.7	367.4	1	0.8	380

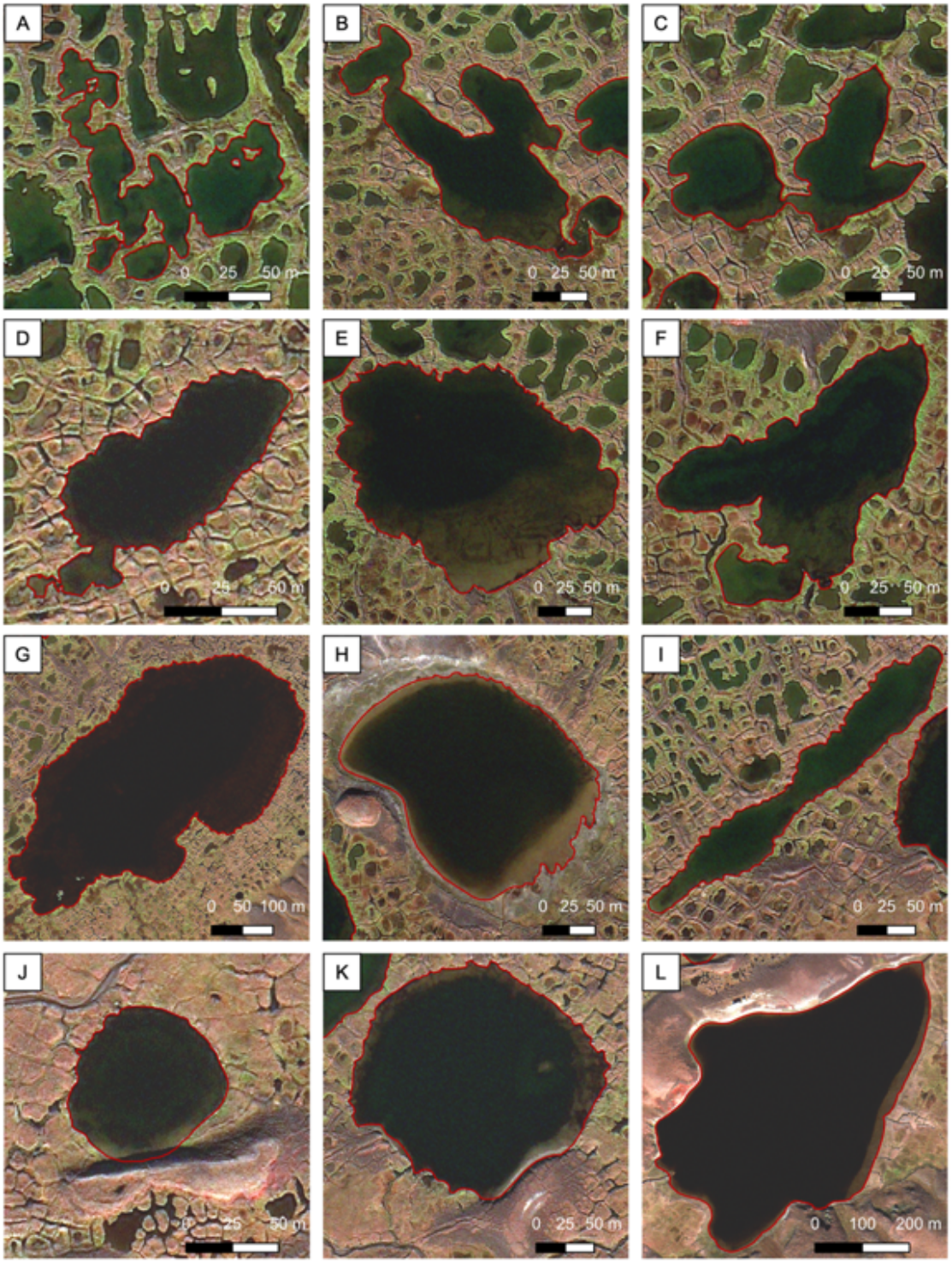

Figure S4: Satellite images of lakes (A to U; background: GeoEye, 2010).

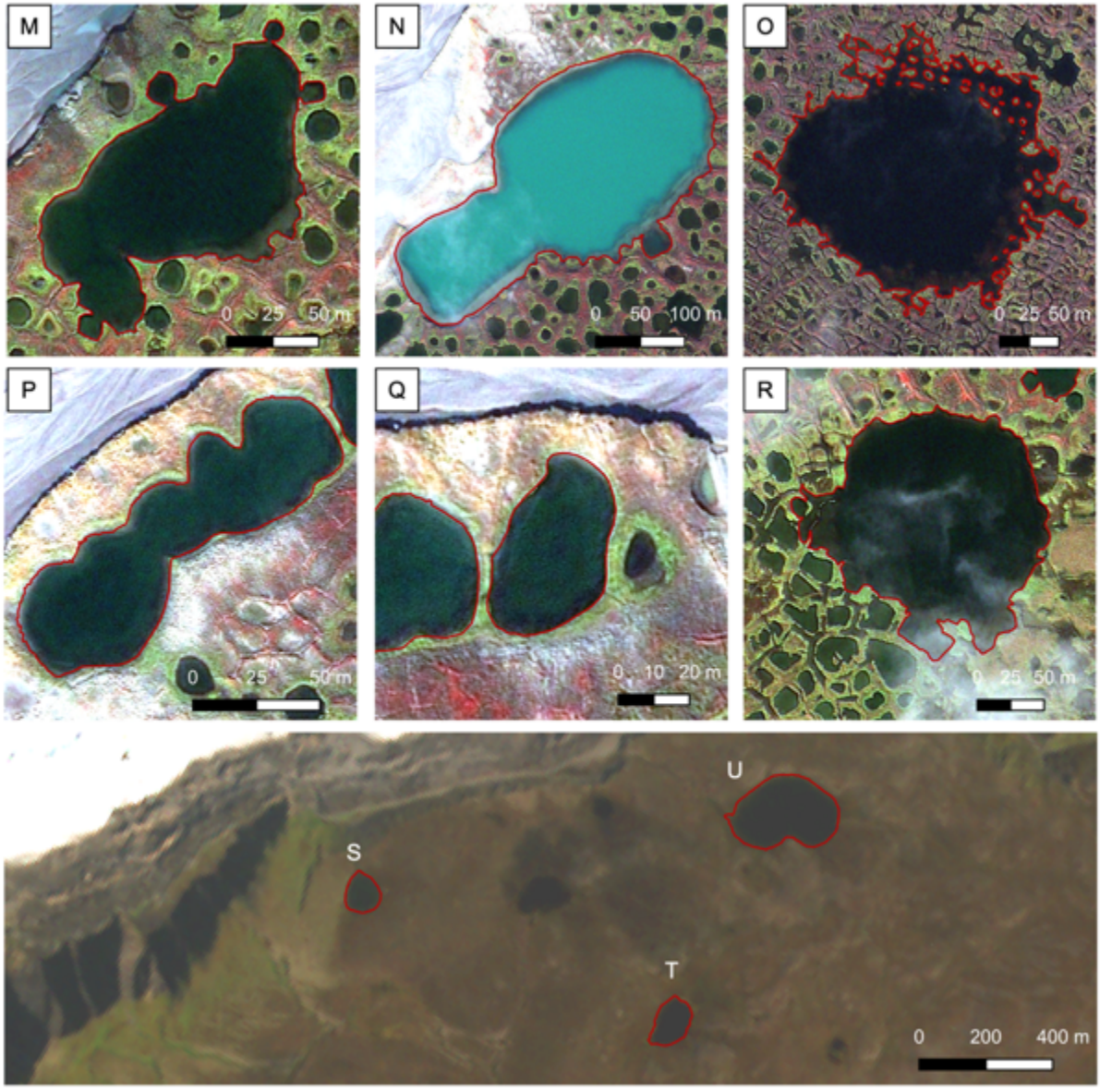

Figure S4 : Continued